Earthq Eng & Eng Vib (2008) 7:369-382 **DOI**: 10.1007/s11803-008-1009-2

Effects of structural characterizations on fragility functions of bridges subject to seismic shaking and lateral spreading

Jian Zhang†, Yili Huo‡, Scott J. Brandenberg† and Pirooz Kashighandi‡

Department of Civil and Environmental Engineering, University of California, Los Angeles, CA 90095, USA

Abstract: This paper evaluates the seismic vulnerability of different classes of typical bridges in California when subjected to seismic shaking or liquefaction-induced lateral spreading. The detailed structural configurations in terms of superstructure type, connection, continuity at support and foundation type, etc. render different damage resistant capability. Six classes of bridges are established based on their anticipated failure mechanisms under earthquake shaking. The numerical models that are capable of simulating the complex soil-structure interaction effects, nonlinear behavior of columns and connections are developed for each bridge class. The dynamic responses are obtained using nonlinear time history analyses for a suite of 250 earthquake motions with increasing intensity. An equivalent static analysis procedure is also implemented to evaluate the vulnerability of the bridges when subjected to liquefaction-induced lateral spreading. Fragility functions for each bridge class are derived and compared for both seismic shaking (based on nonlinear dynamic analyses) and lateral spreading (based on equivalent static analyses) for different performance states. The study finds that the fragility functions due to either ground shaking or lateral spreading show significant correlation with the structural characterizations, but differences emerge for ground shaking and lateral spreading conditions. Structural properties that will mostly affect the bridges' damage resistant capacity are also identified.

Keywords: fragility functions; bridge; seismic response; liquefaction; lateral spreading; structural characterization

1 Introduction

Highway bridges are the most common type of bridge and are crucial components of transportation networks. They are susceptible to damage under major earthquakes, which subsequently cause threat to human safety, and result in significant direct or indirect economic impact. Two significant mechanisms of damage observed in past earthquakes are seismic shaking and liquefaction-induced lateral spreading. Increased horizontal and vertical load due to dynamic effects under seismic shaking is attributed as the most dominant cause of bridge damage observed in past earthquakes (Priestley *et al*., 1996; Basöz and Kiremidjian, 1998). The column failure experienced by the Hanshin expressway during the 1995 Kobe earthquake (Kawashima and Unjoh, 1997) and bridge collapse of the Cypress Street Viaduct during the 1989 Loma Prieta earthquake (Chen and Duan, 2003) are examples of failures caused by excessive seismic loading. For bridges built on liquefiable soil, earthquake-induced liquefaction and lateral spreading have significant impact on foundation weakening/failure and subsequent structural damage. The span unseating of the Nishinomiya Bridge during the 1995 Kobe earthquake (Wilson, 2003) and collapse of the Showa Bridge during the 1964 Niigata earthquake (Yasuda and Berrill, 2000) are examples of spectacular failures caused by liquefaction. Nevertheless, there are many bridges that have performed reasonably well under either seismic shaking or lateral spreading. For example, the Landing Road Bridge suffered only moderate and reparable damage despite as much as 2.0 meters of lateral spreading of the surrounding soils during the 1987 Edgecumbe earthquake (Berrill *et al*., 2001). It is observed that the detailed structural configurations (e.g., column detailing, superstructure type, material, connection, continuity at support and foundation type, etc.) render different damage resistant capability for bridges. Furthermore, the failure mechanisms of bridges exhibited by seismic shaking or liquefaction-induced lateral spreading inevitably show different patterns due to distinct load transferring mechanisms, resulting in differences in damage potential under these two situations. Therefore, it is important to evaluate the damage potential of different classes of bridges under seismic shaking and liquefaction-induced lateral spreading so that sound judgment can be made in terms of choosing appropriate design or retrofit measures to

Correspondence to: Jian Zhang, Department of Civil and Environmental Engineering, University of California, Los Angeles, CA 90095, USA
Tel: (310) 825-7986; Fax: (310) 206-2222
E-mail: zhangj@ucla.edu
†Assistant Professor; ‡Graduate Student Researcher

Supported by: Pacific Earthquake Engineering Research Center Lifelines Program Under Project Task No. 9C
Received October 29, 2008; **Accepted** November 3, 2008

improve bridge response during earthquakes.

There are inherent variabilities and uncertainties associated with the seismic responses of bridges due to either shaking (e.g., structural properties, earthquake motion characteristics, etc.) or liquefaction and liquefaction-induced lateral spreading (e.g., structural properties, soil properties, liquefaction mechanism and ground movement, etc.). The deterministic seismic analysis approaches are not able to account for these inherent variabilities and uncertainties. Under a probabilistic framework, this paper adopts the fragility function method to provide a comprehensive evaluation of bridge response and damage potential under seismic shaking and lateral spreading loading conditions. Fragility functions, which relate the damage probability of bridges to either the intensity measure of earthquake input motions (e.g., peak ground acceleration) or liquefaction-induced ground displacement, are generated and compared for six types of typical highway bridges in California in order to evaluate the effects of structural characterizations on the damage probability of bridges. Nonlinear dynamic time history analyses are used to derive the fragility functions of bridges under seismic shaking while equivalent static procedure is used to derive the fragility functions of bridges under liquefaction-induced lateral spreading. The important structural and foundation parameters are also identified. The study provides a comprehensive evaluation of bridge response under earthquakes.

2 Responses of bridges under seismic shaking

2.1 Methodology of fragility analysis

Fragility functions are useful tools for assessing the seismic vulnerability of highway bridges in terms of prioritizing retrofit, pre-earthquake planning and post-earthquake loss estimation. Fragility functions define the conditional probability of attaining or exceeding a specified damage state for a given set of input intensity measures or engineering demand parameters. Depending on different data resources, fragility functions can be generated as empirical ones with observed damage data from past earthquakes (Basöz *et al*., 1999; Yamazaki *et al*., 2000) and analytical ones based on the results of numerical analyses. Analytical fragility functions are developed using seismic response data of bridges obtained from nonlinear time history analysis, elastic spectra analysis or nonlinear static analysis (Choi *et al*., 2004). Reasonably good agreement is obtained between the analytical and empirical fragility functions (Shinozuka *et al*., 2000).

This paper employs the probabilistic seismic demand model (PSDM) to derive analytical fragility functions of bridges under seismic shaking using nonlinear time history responses. The PSDM can be developed using a 'scaling' approach or 'cloud' approach (Baker and Cornell, 2006) to relate the engineering demand parameters (EDPs), D_D, to the ground motion intensity measures (IMs), I_M. With the 'scaling' approach, all motions are scaled to selective intensity levels corresponding to prescribed seismic hazard levels and incremental dynamic analysis is performed at different hazard levels. On the other hand, the 'cloud' approach uses unscaled earthquake ground motions. In this paper, the 'cloud' approach is termed as PSDA (Probabilistic Seismic Demand Analysis) while the 'scaling' approach is termed as IDA (Incremental Dynamic Analysis). The PSDA method utilizes regression analysis to obtain the mean and standard deviation for each limit state by assuming a logarithmic correlation between median engineering demand D_D and an appropriately selected intensity measure I_M:

$$D_D = a\left(I_M\right)^b \quad \text{or} \quad \ln\left(D_D\right) = \ln a + b\ln\left(I_M\right) \tag{1}$$

where the parameters a and b are regression coefficients obtained from the response data of nonlinear time history analyses. The remaining variability in ln (D_D) at a given I_M is assumed to have a constant variance for all I_M range, and the standard variation is estimated as (Baker and Cornell, 2006):

$$\xi_{EDP|IM} = \sqrt{\frac{\sum_{i=1}^{n}\left[\ln\left(D_{Di}\right) - \left(a + b\ln I_{Mi}\right)\right]^2}{n-2}} \tag{2}$$

Subsequently, the EDPs are converted to the damage index (DI), D_I that is compared with the limit states (LS), L_S corresponding to various damage states (DS), D_S, dictated by a capacity model. If the D_I is the same as the D_D, by further assuming a log-normal distribution of D_D at a given I_M, the fragility functions (i.e., the conditional probability of reaching a certain damage state for a given I_M) are written as:

$$P\left[D_I \geq L_S \,|\, I_M\right] = 1 - \int_0^{L_S} \frac{1}{\sqrt{2\pi}\cdot\xi_{EDP|IM}\cdot d_d}\cdot \exp\left\{-\frac{\left[\ln\left(d_d\right) - \ln\left(a\cdot {I_M}^b\right)\right]^2}{2\left(\xi_{EDP|IM}\right)^2}\right\}\mathrm{d}\left(d_d\right) \tag{3}$$

where $\xi_{EDP|IM}$ is the standard deviation of simulation data from the logarithmic correlation between median D_D and I_M. It is obtained from Eq. (2).

In contrast to the PSDA method, the IDA method requires more computational effort because of the scaling of earthquake motions to different intensity levels, i.e., through increments. However, no a priori assumption needs to be made in terms of probabilistic distribution of seismic demand in order to derive the fragility curves. Nonlinear time history analysis will be conducted at every intensity level. The occurrence ratio

of a specified damage state is computed and directly used as the damage probability at the given I_M level, i.e., the damage probability is calculated as the ratio of the number of damage cases n_i at and beyond the damage state i over the number of total simulation cases N at a given I_M level (Karim and Yamazaki, 2001):

$$P\left[D_I \geq L_{Si} \middle| I_M\right] = \frac{n_i}{N} \qquad (i = 1 \text{ to } 4) \tag{4}$$

In most cases, IDA fragility curves can be fitted with either a normal cumulative distribution function:

$$P[D_I \geq L_S \mid I_M] = \int_{-\infty}^{I_M} \frac{1}{\sqrt{2\pi}\sigma_{IM}} \exp\left[-\frac{(i_m - \mu_{IM})^2}{2\sigma_{IM}^2}\right] \mathrm{d}(i_m) \tag{5}$$

or a log-normal cumulative distribution function:

$$P[D_I \geq L_S \mid I_M] = \int_0^{I_M} \frac{1}{i_m \sqrt{2\pi}\xi_{IM}} \exp\left\{-\frac{\left[\ln(i_m) - \lambda_{IM}\right]^2}{2\xi_{IM}^2}\right\} \mathrm{d}(i_m) \tag{6}$$

where σ_{IM} and μ_{IM} are standard deviation and mean value of IM to reach the specified damage state based on the normal distribution while ξ_{IM} and λ_{IM} are standard deviation and mean value of ln (I_M) to reach the specified damage state based on the log-normal distribution.

2.1.1 Earthquake selection and intensity measure

Since both PSDA and IDA methods rely on a large number of nonlinear time history analyses to derive the fragility functions, a significant number of earthquake records need to be selected so that a conceptually and statistically better prediction of bridge response can be obtained. In this paper, 250 sets of earthquake ground motion records are selected from the PEER strong motion database (http://peer.berkeley.edu/smcat) and the records are applied in transverse, longitudinal and vertical directions simultaneously in the time history analysis. Figure 1 shows the distribution of peak ground acceleration (PGA), A_{PG}, peak ground velocity (PGV), V_{PG}, spectral acceleration, S_a, at period T=0.5 s, earthquake magnitude M and distance to epicenter r as well as the site conditions of the selected ground motion records. The site conditions are characterized based on

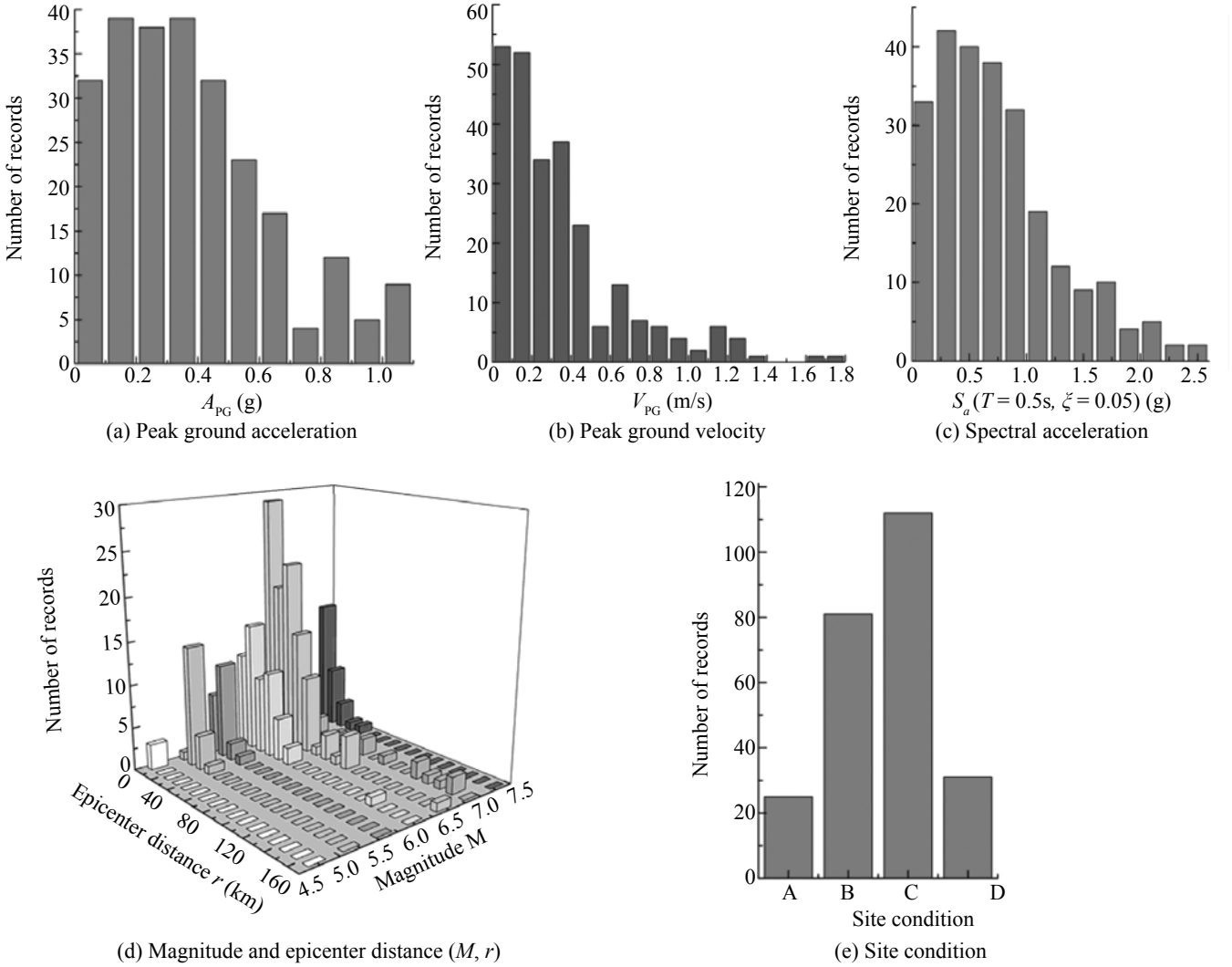

(a) Peak ground acceleration (b) Peak ground velocity (c) Spectral acceleration

(d) Magnitude and epicenter distance (M, r) (e) Site condition

Fig. 1 Characteristics of selected earthquake ground motion records (horizontal component)

the average shear wave velocity to a depth of 30 m according to USGS site classification criteria.

The ground motions are characterized by the intensity measure I_M and the choice of I_M plays a crucial role both in running the fragility analysis and interpreting simulation results. Peak ground acceleration A_{PG} is adopted as I_M for earthquake input in this study based on the linear consistency criterion suggested by Mackie and Stojadinović (2003) and with the consideration of its efficiency, practicality and hazard computability as discussed by Padgett *et al*. (2008).

2.1.2 Damage index and limit states

The seismic responses of bridges are depicted and monitored by EDPs. Subsequently, the EDPs are related to the damage index D_I for various damage states D_S using their corresponding limit states L_S based on physical phenomenon or theoretical judgment. The fragility function method generally classifies the damage into four levels: slight, moderate, extensive and collapse damage, which can, respectively, be pointed as damage states D_S 1, 2, 3 and 4. For conventional highway bridges, columns are the most critical component and are often forced into the nonlinear range under strong earthquake shaking. A number of studies have developed the criteria for D_I and corresponding L_S based on damage status or loss of load-carrying capacity. Commonly used D_I measures for columns are curvature ductility, displacement ductility and residual displacement, etc., and four damage states defined by HAZUS (FEMA, 2007) are usually adopted. In this study, the curvature ductility μ_κ is adopted as D_I for columns and the corresponding L_S values are those adopted by Choi *et al*. (2004). For bridges with seat-type abutments or isolation devices, the bearings will experience large displacements resulting in damage of isolation devices and neighboring structural members in addition to the possible damage in columns. The damage states of isolation devices are determined based on experimental observation as well as consideration of the resulting pounding and unseating. Typically, either the bearing displacement or shear strain is used to describe the damage states. In this study, generic isolation bearings with mechanical properties resemble to that of lead rubber bearings are used at the seat-type abutments and pier tops (if applicable) and the shear strain is utilized to capture the damage states in bearings. Table 1 lists the engineering demand D_D, damage index D_I, damage state D_S and corresponding limit state L_S definitions for these two components. Although modern isolation bearings can experience shear strains up to 400% before failure, such large shear strains will be the result of large lateral displacements which will be prevented by pounding at the abutment or preceded by girder unseating. Therefore, a maximum 250% shear strain is adopted in this study, which corresponds to 0.25 m maximum displacement.

During earthquake shaking, piers and bearings can exhibit different component damage states that are combined into a comprehensive damage state for the bridge system, which is hard to describe by only one component damage index D_I. Previous studies suggest that a system fragility can be derived based on functionality or repair cost after an earthquake (Mackie and Stojadinović, 2007), or can be generated based on component level fragility functions (Nielson and DesRoches, 2007). In this study, a composite damage state (D_S) is devised as shown in Eq. (7). The proportion ratio 0.75 for columns and 0.25 for bearings are determined synthetically by considering the relative component importance for load-carrying capacity during earthquake and the repair cost after earthquake.

$$D_S^{\mathrm{System}} = \begin{cases} \mathrm{int}\left(0.75D_S^{\mathrm{Pier}} + 0.25D_S^{\mathrm{Bearing}}\right) & D_S^{\mathrm{Pier}},\ D_S^{\mathrm{Bearing}} < 4 \\ 4 & D_S^{\mathrm{Pier}} \text{ or } D_S^{\mathrm{Bearing}} = 4 \end{cases} \tag{7}$$

Table 1 Definition of component level damage index of columns and bearings

Component	D_D or D_I definition	Slight (D_S= 1)	Moderate (D_S= 2)	Extensive (D_S= 3)	Collapse (D_S= 4)
Columns (Choi *et al*., 2004)	Section ductility μ_k	μ_k >1	μ_k > 2	μ_k > 4	μ_k > 7
Bearings	Shear strain γ	γ > 100 %	γ > 150 %	γ > 200 %	γ > 250 %

2.2 Bridge types and numerical modeling

The typical bridge designs are evaluated by reviewing the drawings of numerous bridges obtained from the California Department of Transportation (Caltrans) and six bridge models, as shown in Fig. 2, are selected to represent the most common highway bridge types. These models represent the different variations of a multi-span straight bridge with single column construction. The bridge with pier bent (i.e., multiple columns), though not considered in this paper, is another common type of construction in California. Model E1 represents a continuous bridge with monolithic abutments. In contrast to model E1, models E2-E6 all have seat-type abutments where isolation bearings are used. Model E2 represents a continuous bridge with seat-type abutments. Model E3 is similar to Model E2 except that it has an expansion joint at the center of the mid-span. Model E4 is also isolated at the pier tops with continuous deck, while model E5 has an expansion joint at the mid-span in addition to the isolation. In model E6, simply supported connections are adopted at the column top and the adjacent decks are pin

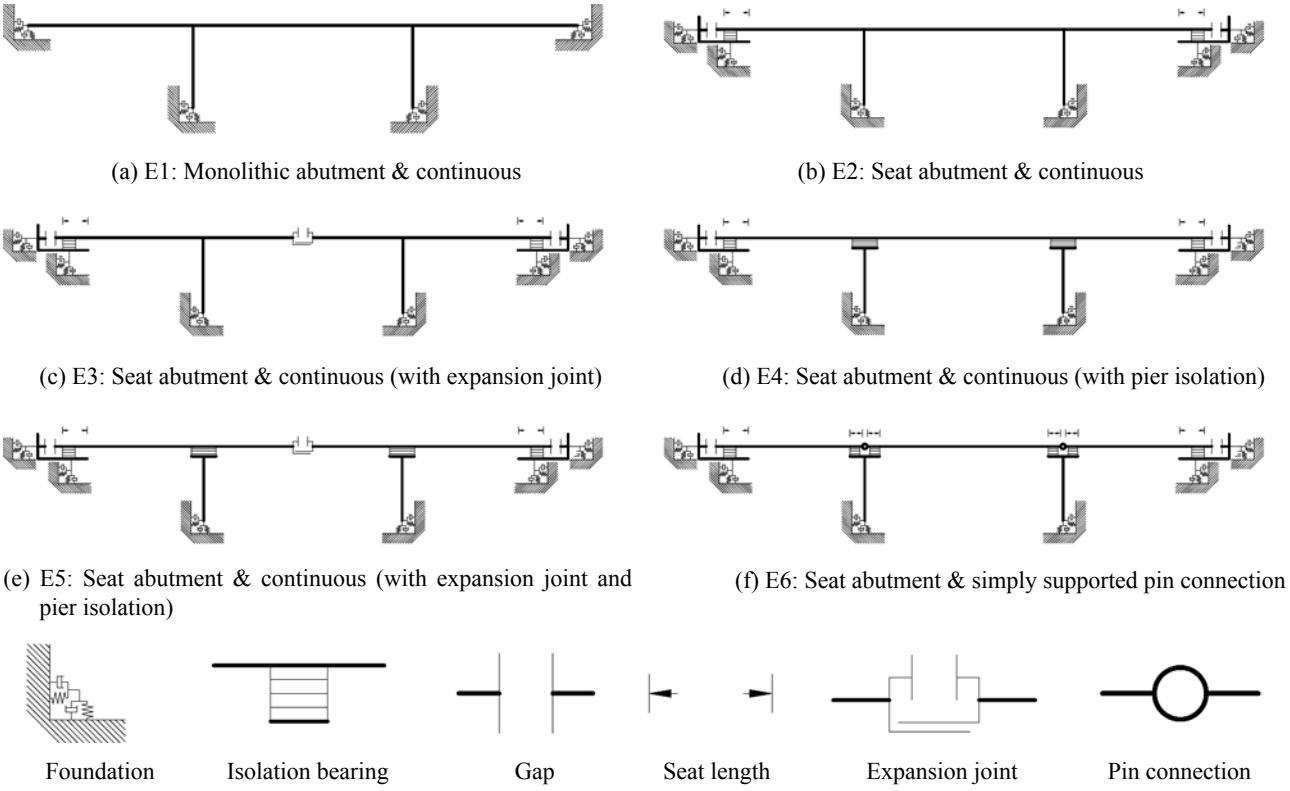

Fig. 2 Sketches of the six bridge models

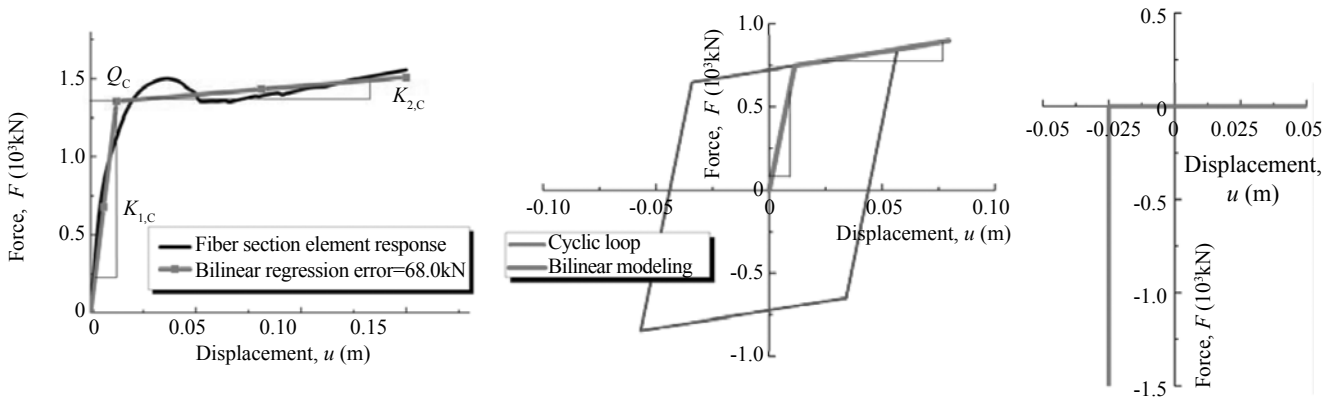

(a) Column (b) Isolation bearing (c) Gap

Fig. 3 Force-displacement relationships of column, isolation bearing and gap element

Table 2 Bridge component properties and modeling parameters

	Deck	Columns	Bearings	Gaps
Properties	Box girder with spans of 20 m/30 m/20 m	Circular section (d = 72in) with 26#11 (longitudinal) and #4@12 in (transverse) reinforcement (1 in = 0.0254m)	Elastomeric rubber bearing for seat-type abutments and isolation at top of pier	Gap distance: 0.025m
Modeling and parameters	Elastic beam elements	Fiber section beam elements $K_{1,C}=1.10\times10^5$ kN/m $Q_C=1.36\times10^3$ kN	Bilinear (horizontal) and linear (vertical) springs. $Q_B=0.55Q_C$ $K_{1,B}=0.60K_{1,C}$ $K_{2,B}=K_{1,B}/30$	Gap elements: $\Delta_y=-0.025$ m

connected to prevent collapse. The structural properties of bridge components are taken from two real Caltrans bridges that were built before 1971, and are therefore characteristic of older-vintage bridges designed before adoption of modern seismic codes. A previous study (Zhang *et al*., 2008) has shown that the location of expansion joints, if kept in a reasonable and practical range, has no obvious effect on the seismic response of bridges with straight alignment and symmetrical geometry, so in this study its location is not varied.

Numerical models were generated in software platform OpenSees (documented by Mazzoni *et al*., 2006). Elastic beam elements are used for the bridge deck and nonlinear fiber section beam elements are used to model the columns. The RC column has 72 in (1 in = 0.0254 m). diameter and is reinforced with 26#11 longitudinal bars and #4 transverse reinforcements at 12 in. intervals. Figure 3(a) plots the force-displacement relationship of a single column from the push-over analysis using fiber elements in OpenSees. The force-displacement relationship of the column can be roughly approximated with a bilinear regression curve. Hence the column has an elastic stiffness of $K_{1,C}$=1.10×10^5 kN/m and characteristic strength of Q_C=1.36×10^3 kN as indicated by the bilinear curve. This represents a typical design for bridges built before 1971. The middle span is 30 m long while the other two spans are 20 m each. Seismic isolation bearings are modeled with bilinear springs for horizontal load-carrying properties and elastic springs for vertical properties (Kumar and Paul, 2007). The bearing parameters are selected based on the optimum design parameters as presented in Zhang and Huo (2008). Figure 3(b) plots the force-displacement relationships of the bearing and its modeling parameters, $K_{1,B}$, $K_{2,B}$ and Q_B. Gap elements are employed to simulate the gap closing and the effects of pounding between deck and abutment. Figure 3(c) shows the force-displacement relationship of the gap element with a 1 in.opening. The seat length (maximum 0.25 m) during earthquake shaking and lateral spreading is monitored and the analysis will be terminated if the seat length is reduced to zero, i.e., the unseating is impending. The soil-structure interaction (SSI) is simulated with springs and dashpots representing the stiffness and damping of foundations supporting columns and embankment at end abutments, whose properties are determined by the methods presented by Zhang and Makris (2002a, b). Table 2 summarizes the properties and modeling parameters of key bridges components.

2.3 Fragility functions of bridges under seismic shaking

2.3.1 Fragility functions of model E1

The model E1 is studied first as an example to demonstrate the implementation of PSDA and IDA methods. With the PSDA method, Fig. 4(a) shows the data points of the computed section curvature κ (rad/m) (D_D) versus the corresponding PGA (I_M) of unscaled ground motions in logarithmic scale, and a linear regression which provides a reliable relationship between I_M and D_D and an estimation of the standard deviation. Based on Eqs. (1) and (2), the parameters of the regression are obtained as a=0.00331 and b=1.866 while the dispersion (i.e., the standard deviation of the distribution) is computed as $\xi_{EDP|IM}$=0.360. With Eq. (3), the fragility data at each A_{PG} level of the specified damage state could be calculated and the fragility functions are then derived with these data, as shown in Fig. 4(b).

With the IDA method, the 250 sets of records are scaled to 25 A_{PG} levels from 0.06 g to 1.50 g with 0.06g increments. The fragility functions are then derived following Eq. (4) with the data from 6250 (250 × 25) nonlinear dynamic analyses. Figure 5(a) shows the 'raw' fragility curves and the regression curves generated using cumulative normal (Eq. (5)) or lognormal (Eq. (6)) distribution functions. Both normal and log-normal distributions yield similar results compared to

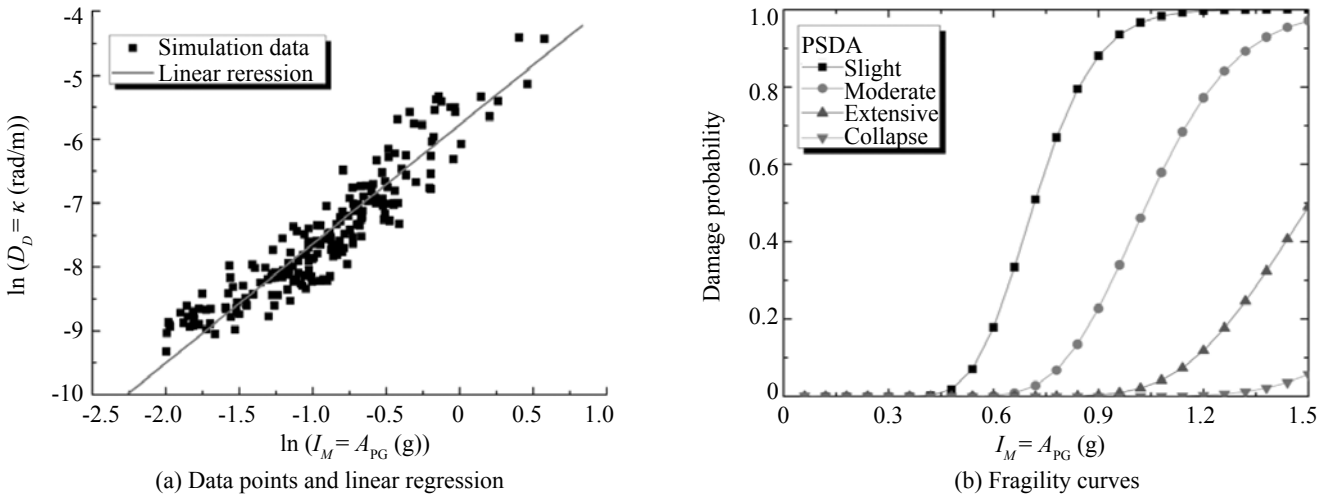

(a) Data points and linear regression

(b) Fragility curves

Fig. 4 PSDA fragility analysis of Model E1

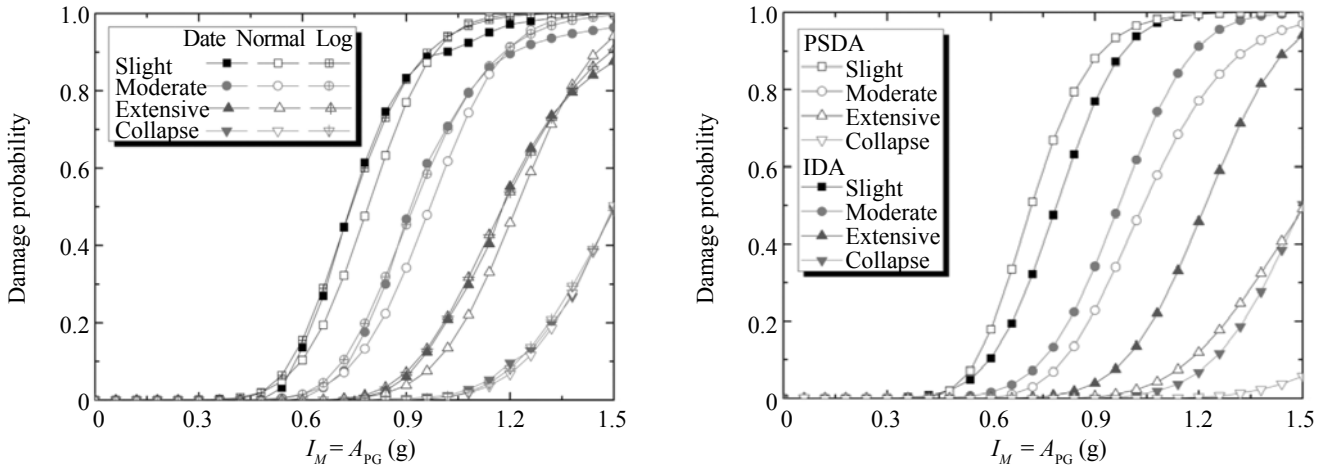

(a) IDA fragility curves and regression

(b) Comparison of PSDA and IDA

Fig. 5 Fragility functions of Model E1 using PSDA and IDA methods

the raw data. Figure 5(b) compares the fragility curves generated by the PSDA and IDA methods, respectively. It is seen that the two methods yield comparable results at slight and moderate damage states, but different results for extensive and collapse states. It is noted that the IDA method is generally more reliable than the PSDA method because the fragility functions are based on many more simulation cases and no pre-adopted relationship between the EDP and IM is assumed, although some possible bias from the record scaling process has been pointed out by previous studies (Luco and Bazzuro, 2007). Some errors or bias are introduced into the PSDA method due to a single assumption relating EDP to IM despite the damage states. In particular, the lack of large intensity earthquake motion records (as shown in Fig. 1) may introduce some error to the PSDA results as the input motions are biased toward smaller intensity. This imbalance results in the discrepancy between PSDA and IDA methods observed in Fig. 5(b).

2.3.2 Fragility functions of different bridge types

With the consideration of the possible bias of PSDA, the following analyses utilize the IDA method to generate fragility curves for all six bridge models shown in Fig. 2. Figure 6 compares the fragility curves of six different bridge models considered in this study for slight, moderate, extensive and collapse damage states. The results show that models E2 and E3 perform the least favorably among the six bridge types shown in Fig. 2. The more severe damage in models E2 and E3 is attributed to the seat-type connection at abutments, which leads to smaller dynamic loads carried at abutments, resulting in more loads being transferred to columns. In contrast to the seat-type abutment, the isolation bearings at the pier top reduces the damage experienced by the columns, which is reflected by much lower fragility curves of models E4 and E5 than for models E2 and E3. The expansion joint of model E3 does not make much difference in terms of the bridge response compared to model E2. A similar trend is seen between models E4 and E5 for slight and moderate damage states. However, the expansion joint makes the isolated bridge more vulnerable to extensive and collapse damages, possibly due to the pounding between adjacent segments. Among all the models, it is seen that model E1 performs the best for smaller earthquake intensities (i.e., PGA smaller than 0.7 g for slight and moderate damage states and 1.0 g for the extensive damage state) while model E6 performs the best for higher earthquake intensities for slight, moderate and extensive damage states. The simply-supported connection in model E6 prominently reduces the seismic energy transfer from the deck to the column, hence protecting the column from larger damage potential. The pin connection also limits the extreme bearing damage and span collapse under larger earthquakes. Both factors contribute to the superior performance of model E6 under larger earthquakes. At the collapse damage state, model E1 (a continuous bridge with integral abutments) is clearly the best structural type. Figure 6 shows that the structural characterizations of bridges play an important role in defining the damage potential of bridges under earthquakes.

3 Responses of bridges under liquefaction-induced lateral spreading

3.1 Procedure to simulate bridge response subject to lateral spreading

Liquefaction is defined as a loss of soil strength and stiffness due to the generation of excess pore water pressure. Earthquakes most commonly liquefy loose, saturated sands. Liquefaction can trigger ground deformations due to loss of strength combined with transient inertial stresses induced by ground shaking and any static driving shear stresses. Flow liquefaction occurs when the shear stresses required for static equilibrium

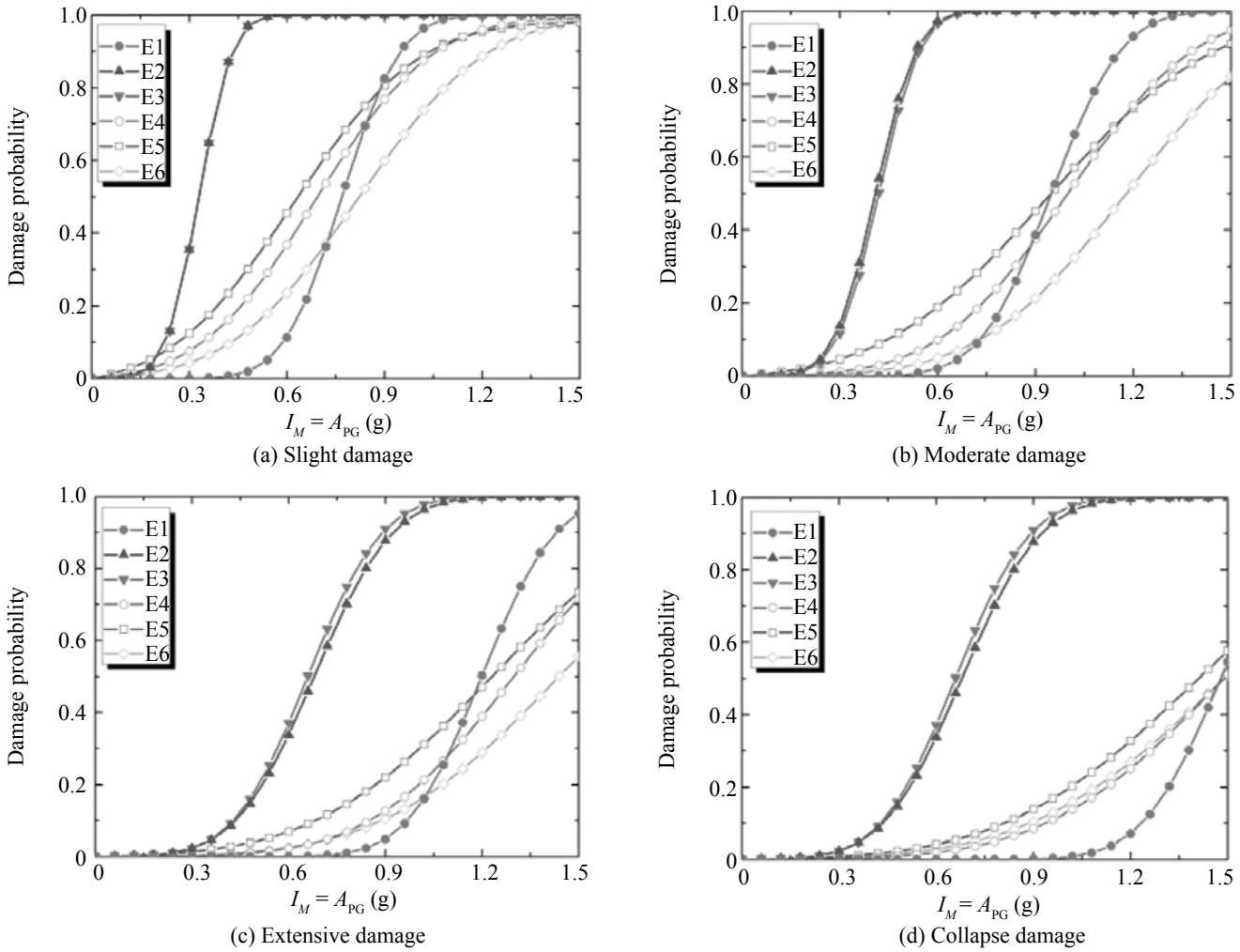

Fig. 6 Fragility curves of six bridge models under seismic shaking

of a soil mass are greater than the shear strength of the liquefied soil, which can lead to large deformations on the order of many meters. Cyclic mobility occurs when the initial static stresses are less than the strength of the liquefied soil, but transient stresses during shaking exceed the material strength causing an accumulation of displacements. Liquefaction-induced lateral ground displacement up to a couple of meters is often called lateral spreading. Embedded bridge components can attract large lateral loads from laterally spreading soil, particularly when a non-liquefied crust spreads laterally on top of underlying liquefied layers.

Due to extraordinary difficulties both in theoretical and computational efforts involved in three-dimensional continuum finite element modeling, the dynamic simulation of the liquefaction and lateral spreading process, which is intuitively appropriate, is not feasible for bridge fragility analysis. Instead, an equivalent static analysis procedure proposed by Brandenberg *et al*. (2007b) is employed to simulate the bridge response under liquefaction-induced lateral spreading. In this procedure, free-field lateral spreading demands are imposed as displacements on the free ends of *p-y* springs attached to the bridge foundation, as shown in Fig. 7. Inertia forces can occur simultaneously with lateral spreading forces, and are imposed on the superstructure at connections with the piers and abutments, and also at the pile caps. The imposed inertia forces are consistent with the imposed free-field lateral spreading displacements based on a Newmark sliding block method (Brandenberg *et al*., 2007a). By analogy with the Incremental Dynamic Analysis method presented in the previous section, this analysis approach for lateral spreading is considered an "Incremental Static Analysis" since free-field ground displacements are incrementally increased while the bridge damage is monitored.

The above six models in seismic shaking analysis are also evaluated for their performance under the liquefaction-induced lateral spreading. They are labeled as models P1 to P6 in order to distinguish the differences in foundation modeling from models E1 to E6. All superstructure properties of models P1 to P6 are kept the same as in models E1 to E6, respectively. However, the pile foundations are modeled by bilinear beam elements on a Winkler foundation with *p-y, t-z* and *q-z* spring elements to simulate the soil lateral

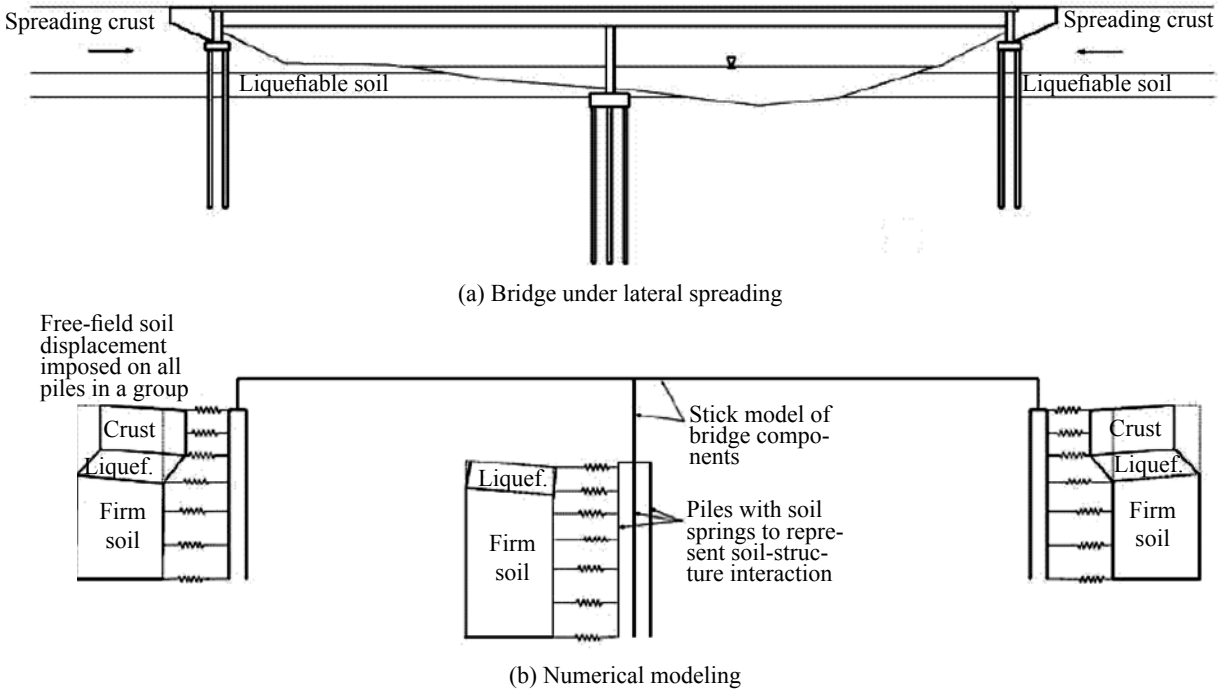

Fig. 7 Numerical modeling of lateral spreading to bridges

resistance, axial shaft friction and pile tip end bearing resistance, respectively. The soil profile used in this study is representative of sites with a non-liquefiable clay crust over liquefiable loose sand over non-liquefied dense sand. Variations in the soil parameters were based on the USGS database of CPT soundings in the San Francisco bay area (USGS, 2007). Figure 8 presents the sketch of a bridge founded on the soil profile. The layer properties and lateral spreading parameters used in this study are listed in Table 3 (as the median values). From the information on soil profile, the properties of *p-y* elements are determined based on a non-liquefied soil profile and subsequently modified to account for the effects of liquefaction by (1) softening and weakening the *p-y* elements in the liquefied sand layer using a p-multiplier, and (2) softening (but not weakening) the *p-y* elements in the non-liquefiable crust layer to account for the influence of the underlying liquefied sand using models derived by Brandenberg *et al*. (2007a). Softening of the *p-y* elements using this method indirectly accounts for the pinning effects of the bridge components on the spreading soils by coupling Newmark sliding block analyses with the load transfer behavior. Pinning effects are considered more rigorously in other studies (e.g., Martin *et al*., 2002; Boulanger *et al*., 2005).

Figure 9 presents the deformed shape of bridge model P1 under two possible load cases for liquefaction-induced lateral spreading. The results were obtained by imposing the displacements on the free ends of the *p-y* elements to model lateral spreading demands. In load case I (Fig. 9(a)), lateral spreading happens in the left embankment and left pier foundation. Although the displacement load of lateral spreading is applied on the left side of the bridge, it is the right column that

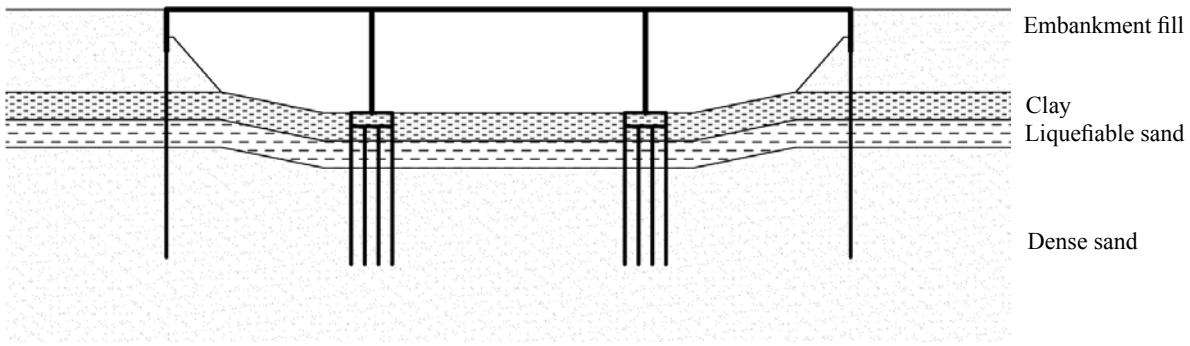

Fig. 8 Sketch of simulation for bridge and soil profile with liquefiable sand layer

experiences larger deformation and therefore more severe damage in this loading case. This is due to the left-to-right displacement of the entire bridge, which acted like a system to the imposed spreading demands. In load case II (Fig. 9(b)), only the left pier foundation experiences lateral spreading displacement load. The analysis results show that the left column suffers the most damage of the bridge but the damage is much smaller than in load case I given the same displacement magnitude. Figure 9 shows that the location of lateral spreading demands directly affects the bridge response and damage levels. Furthermore, damage is not restricted to the components exposed to liquefaction and lateral spreading, as loads may be shifted to other components in competent soil. Accurately predicting the areal extent of liquefaction and the amount of ground displacement is often difficult, and imposing many different load combinations may be required to identify the most critical conditions for a particular bridge. A procedure is currently under development to assess the influence of various lateral spreading displacement combinations on bridge response.

Variability in soil profiles is included to reasonably capture a range of possible site conditions based on available data and the authors' judgment, as specified in Table 3. Soil properties were sampled from their respective distributions, and each bridge was analyzed using the loading case I shown in Fig. 9. Demands on various bridge components were recorded and related to the damage index. The detailed analysis procedure as well as the sensitivity study on parameters is provided in a related study (Brandenberg *et al*., 2008).

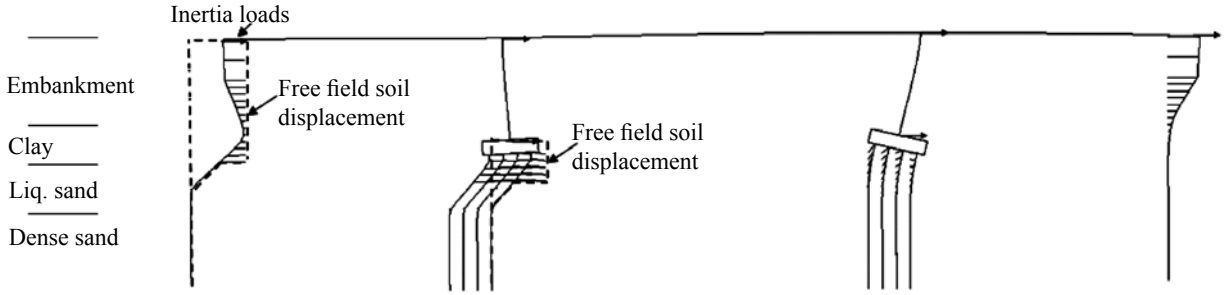

(a) Load case I: Lateral spreading at left abutment and pier

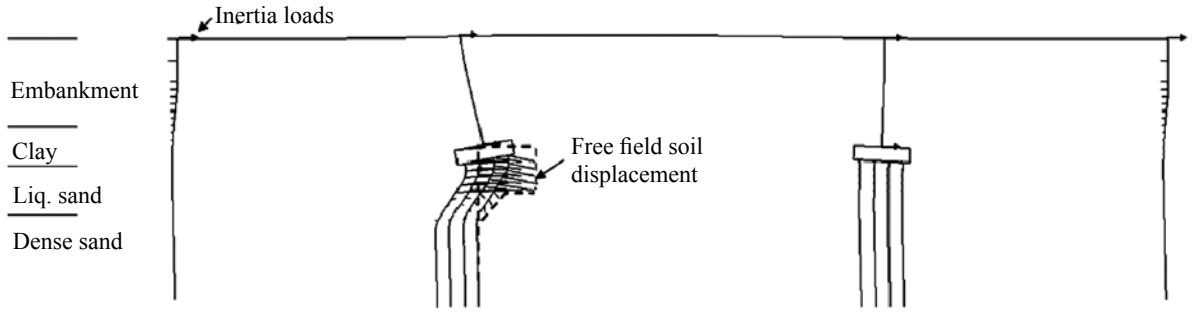

(b) Load case II: Lateral spreading at left pier

Fig. 9 Bridge deformations under two lateral spreading load cases

3.2 Fragility functions of bridges under liquefaction-induced lateral spreading

Corresponding to a static simulation procedure, First Order Second Moment (FOSM) and Monte Carlo methods are generally adopted to generate fragility functions. The FOSM method assumes that both the input properties and output responses follow either normal or log-normal distributions, and applies only first order terms in Taylor's expansion to estimate the mean and standard deviation of response if the mean and standard deviation of the input properties are known (Christian, 2004) as shown below:

$$\mu_M = M\left(\mu_{x_1}, \mu_{x_2}, \cdots, \mu_{x_n}\right), \qquad \sigma_M = \sqrt{\sum_{i=1}^{n}\left(\frac{\partial M}{\partial x_i}\right)^2 \sigma_{x_i}^2} \tag{8}$$

On the other hand, the Monte Carlo method selects a large number of input combinations of stochastic variables from the predetermined distribution, and uses these combinations to compute the distribution of the output response (Christian, 2004). As shown in Table 3, eight separate probabilistic parameters are considered in this study. Figure 10 depicts the fragility curves derived with Monte Carlo and FOSM method for bridges under load case I, expressed as damage probability versus free-field lateral spreading displacement (PGD), D_{PG}. The

Table 3 Probability properties of parameters of soil profile and foundation modeling

Parameter		Median	Negative variation	Positive variation	Distribution
Crust thickness	Embankment	6.0 m	4.5 m	7.5 m	Normal
	In-situ clay	3.0 m	1.5 m	4.5 m	
Material properties and crust strength[1]		φ'_{sand} = 38º c'_{sand} = 20.0 kPa Su_{clay} = 70.0 kPa	Median crust strength × 0.46	Median crust strength × 2.17	Lognormal
$\Delta_{sand}/\Delta_{crust}$[2]		0.5	0.16	0.84	Uniform
Liquefied sand m_p		0.050	0.025	0.075	Normal
y_{50} for *p*-*y* springs in crust	Embankment	y_{50} = 0.20 m	Median × 0.5	Median × 1.5	Normal
	In-situ clay	y_{50} = 0.05 m			
Axial tip capacity (Q_{tip})		1020.0kN per pile	Median × 0.5	Median × 1.5	Normal
Inertia load[3]		a_{max} = 0.4 g	a_{max} = 0.2 g	a_{max} = 0.6 g	Normal
Liquefied sand thickness		2.0 m	1.0 m	4.0 m	Lognormal

Note:[1]Crust strength (P_{ult}) is computed by the procedure in Brandenberg *et al*. (2007a) and is assumed to be log-normally distributed.
[2]$\Delta_{sand}/\Delta_{crust}$ is the ratio between the displacement at the top of the loose sand to the displacement of the crust.
[3]Inertial load was increased linearly to reach a_{max} at 0.5 m of ground displacement, after which it was kept constant.

two methods produce nearly identical median values, while the FOSM approach predicts larger variance. The following study adopts the FOSM method to save computational effort.

The fragility curves of the six models are generated and compared in Fig. 11. It is observed that the sequence of damage potential of the models under lateral spreading conditions is quite different from that under seismic shaking conditions. Among the six models, model P1 performs the worst and model P5 performs the best. Because the static load induced by lateral spreading at abutments and one pier is transferred to the other pier through the deck, the isolation bearings at both abutments and pier tops reduce the loads exerted on the columns, and consequently mitigate the pier damage. The seat-type abutments in models P2 and P3 result in slightly smaller damage probability than model P1. This observation is explained by the different loading mechanism due to lateral spreading. For the loading case I considered, the displacement loads are applied at the ends of left abutment and the left pier foundation. The seat-type abutment limits the maximum load that is transferred from the abutment to the columns resulting in a smaller damage probability for the columns. The isolation bearing at the column top also limits the force being transferred to the columns hence resulting in a smaller damage probability, a conclusion similarly drawn for the seismic shaking. The expansion joint of model P3 does not make much difference in terms of the bridge response compared to model P2. However, the expansion joint in model P5 notably reduces the damage probability under lateral spreading when compared to model P4. This is because the expansion joint offers less constraint compared to the continuous deck and it transfers only the contact forces once the gap is closed. For a similar reason, the model P6 with simply-supported connections incurs more damage into the column and the whole bridge than that of models P4 and P5. Similar to the analysis of the seismic shaking part, the above fragility curves illustrate the effects of structural characterizations on the bridge response due to lateral spreading, although different from the cases under seismic shaking. One important difference to consider when comparing damage due to shaking with that from lateral spreading is that shaking loads are transient, whereas lateral spreading displacements are typically largest at the end of shaking with some locked-in residual value. Hence, gaps at abutments and expansion joints that close due to lateral spreading may remain closed following the earthquake.

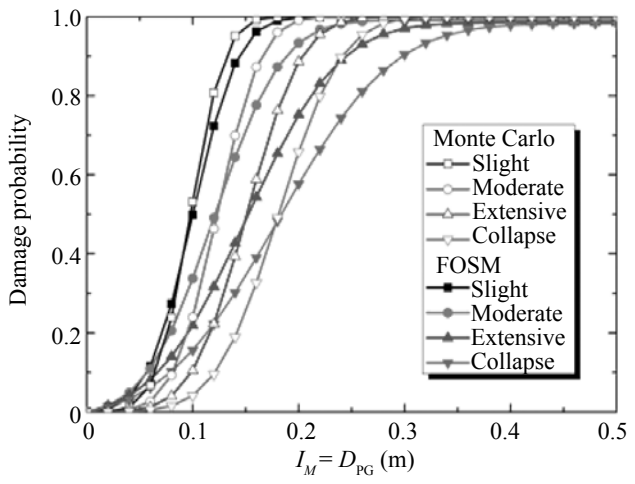

Fig. 10 Fragility curves generated with Monte Carlo method or FOSM

4 Discussion of results

Mean values of the fragility curves μ_{IM} represents the I_M required to reach the specified damage state with 50% probability, and consequently higher μ_{IM} results in lower fragility curves, i.e., better bridge performance. Hence, mean values of fragility functions μ_{IM} could be a good indicator to evaluate the design effectiveness of different structural characterizations. Figure 12 compares the μ_{IM} values of reaching the slight, moderate, extensive and collapse damage states for seismic shaking (Fig. 12(a)) and lateral spreading (Fig. 12(b)) loading conditions. The I_M for the seismic shaking situation is the peak ground acceleration of the input motion while the I_M for the lateral spreading situation is the free-field ground displacement. It is seen that the damage probabilities of different bridge models to seismic shaking and lateral spreading are quite different. Besides, the analyses in previous sections have also demonstrated that structural characterizations may influence bridge response to seismic shaking and lateral spreading in different ways. Seat-type abutments (models E2–E3 and P2–P3) increase the likelihood of bridge damage under seismic shaking, but moderately protects bridges under lateral spreading conditions. Similar effects exist for expansion joints and simply-supported connections. One striking structural property identified in this paper, which is good for both seismic shaking and lateral spreading, is the pier isolation (models E4–E6 and P4–P6). These conclusions could be very valuable for bridge engineers because a bridge designed and retrofitted to resist earthquake shaking may not perform well under liquefaction-induced lateral spreading.

The fragility functions derived in this paper are specific to the structural configurations, ground motions, and soil conditions that have been evaluated, and may not accurately characterize other bridge configurations or loading conditions. For liquefaction and lateral spreading, a strong foundation can potentially resist the lateral spreading demands as the soil fails in the passive mode and spreads around the foundation. In such cases, the bridge damage state will not increase as free-field lateral spreading ground displacement increases, which would be manifested as a flattening out of the fragility curve at a cumulative probability of less than unity. The foundations analyzed in this study were too weak

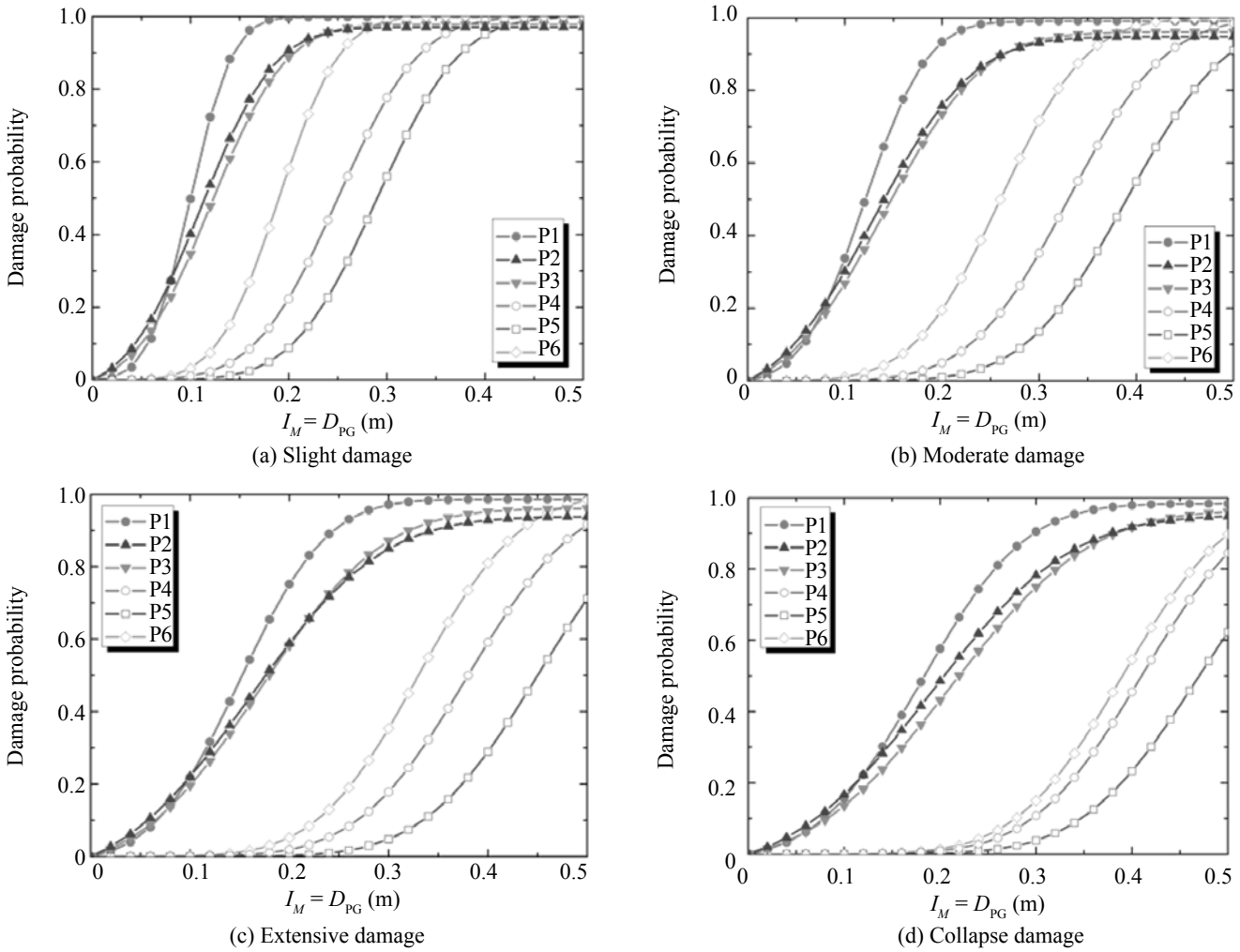

Fig. 11 Fragility curves of six bridge models under lateral spreading

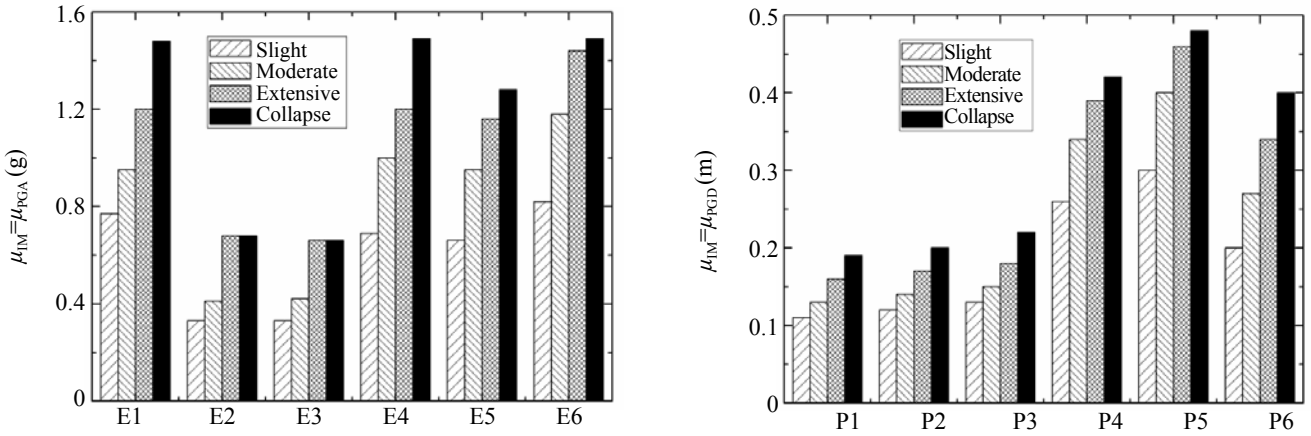

(a) Seismic shaking (b) Lateral spreading

Fig. 12 Mean I_M values for six bridge models to reach various damage states when subject to seismic shaking and lateral spreading

to exhibit this behavior in any significant manner, and bridges with larger-diameter piles or drilled shafts would be anticipated to perform better.

5 Conclusions

In this study, the fragility functions of six different classes of bridges are derived when they are subjected to seismic shaking and liquefaction-induced lateral spreading. The numerical models of bridges and their foundations were built in OpenSees environment to incorporate the soil-structure interaction effects and nonlinear behavior of columns, piles as well as connections. PSDA and IDA approaches are implemented to derive fragility curves under seismic shaking while FOSM and Monte Carlo methods are adopted to generate fragility curves under lateral spreading situation.

The study finds that the fragility functions of bridges subjected to either ground shaking or lateral spreading show significant correlation with the structural characterizations. Under seismic shaking, isolation at the tops of the piers and at the abutments benefits bridge load-carrying capacity, but seat-type abutments make the columns more vulnerable. Furthermore, simply-supported connections reduce the damage in columns and expansion joints do not affect the bridge seismic resistance noticeably. In contrast, under lateral spreading, the isolation at both pier top and seat-type abutments protects columns from damage because a portion of the displacement demand imposed by the spreading soils is accommodated by the isolation components. Expansion joints slightly benefit the bridge response as the gap closing can absorb part of the displacement demand. The simply-supported connection, however, performs less favorably than using continuous deck with isolation on pier tops. In summary, bridges have different resistant capacities to seismic shaking and liquefaction-induced lateral spreading and the differences are explained with the different loading and load carrying mechanisms under these two situations.

Acknowledgement

Funding for this work is provided by the Pacific Earthquake Engineering Research Center Lifelines program under project task No. 9C. The contents of this paper do not necessarily represent a policy of the agency or endorsement by the state or federal government. Tom Shantz and Mark Yashinsky of Caltrans provided valuable help in developing the bridge classification system and providing as-built plans. The research utilizes the Hoffman2 cluster of Academic Technology Services (ATS) at University of California, Los Angeles, to conduct most numerical simulations.

References

Baker JW and Cornell CA (2006), "Vector-valued Ground Motion Intensity Measures for Probabilistic Seismic Demand Analysis," *PEER Report 2006/08*, Pacific Earthquake Engineering Research Center, University of California, Berkeley, CA.

Basöz NI and Kiremidjian AS (1998), "Evaluation of Bridge Damage Data from the Loma Prieta and Northridge, CA Earthquakes," *MCEER Report 98/04*, Multidisciplinary Center for Earthquake Engineering Research, University of California, Berkeley, CA.

Basöz NI, Kiremidjian AS, King SA and Law KH (1999), "Statistical Analysis of Bridge Damage Data from the 1994 Northridge, CA, Earthquake," *Earthquake Spectra*, **15**(1):25–53.

Berrill JB, Christensen SA, Keenan RP, Okada W and Pettinga JR (2001), "Case Study of Lateral Spreading Forces on a Piled Foundation," *Geotechnique*, **51**(6): 501–517.

Boulanger RW, Chang D, Gulerce U, Brandenberg SJ

and Kutter BL (2005), "Evaluating Pile Pinning Effects on Abutments over Liquefied Ground," *Simulation and Performance of Pile Foundations in Liquefied and Laterally Spreading Ground*, Geotechnical Special Publication, ASCE, pp.306–318.

Brandenberg SJ, Boulanger RW, Kutter BL and Chang D (2007a), "Liquefaction-induced Softening of Load Transfer between Pile Groups and Laterally Spreading Crusts," *Journal of Geotechnical and Geoenvironmental Engineering*, **133**(1): 91–103.

Brandenberg SJ, Boulanger RW, Kutter BL and Chang D (2007b), "Static Pushover Analyses of Pile Groups in Liquefied and Laterally Spreading Ground in Centrifuge Tests," *Journal of Geotechnical and Geoenvironmental Engineering*, **133**(9): 1055–1066.

Brandenberg SJ, Kashighandi P, Zhang J, Huo Y and Zhao M (2008), "Sensitivity Study of an Older-vintage Bridge Subjected to Lateral Spreading," *Proceeding of 4th Geotechnical Earthquake Engineering and Soil Dynamics Conference*, Sacramento, USA.

Chen WF and Duan L (2003), *Bridge Engineering: Seismic Design*, NY: CRC Press.

Choi E, DesRoches R and Nielson B (2004), "Seismic Fragility of Typical Bridges in Moderate Seismic Zones," *Engineering Structures*, **26**: 187–199.

Christian JT (2004), "Geotechnical Engineering Reliability: How Well Do We Know What We Are Doing?" *Journal of Geotechnical and Geoenvironmental Engineering*, **130**(10): 985–1003.

Federal Emergency Management Agency (2007), *Multi-Hazard Loss Estimation Methodology, Earthquake Model, HAZUS-MH MR3 Technical Manual*, Washington, D.C.

Karim KR and Yamazaki F (2001), "Effect of Earthquake Ground Motions on Fragility Curves of Highway Bridge Piers Based on Numerical Simulation," *Earthquake Engineering and Structural Dynamics*, **30**: 1839–1856.

Kawashima K and Unjoh S (1997), "The Damage of Highway Bridges in the 1995 Hyogo-Ken Nanbu Earthquake and Its Impact on Japanese Seismic Design," *Journal of Earthquake Engineering*, **1**(3):505–541.

Kumar PTV and Paul DK (2007), "Force-deformation Behavior of Isolation Bearings," *Journal of Bridge Engineering*, **12**(4): 527–529.

Luco N and Bazzurro P (2007), "Does Amplitude Scaling of Ground Motion Records Result in Biased Nonlinear Structural Drift Response?" *Earthquake Engineering and Structural Dynamics*, **36**: 1813–1835.

Mackie K and Stojadinović B (2003), "Seismic Demands for Performance-based Design of Bridges," *PEER Report No.2003/16*, Pacific Earthquake Engineering Research Center, University of California, Berkeley, CA.

Mackie K and Stojadinović B (2007), "Performance-Based Seismic Bridge Design for Damage and Loss Limit States," *Earthquake Engineering and Structural Dynamics*, **36**(13): 1953–1971.

Martin GR, March ML, Anderson DG, Mayes RL and Power MS (2002), "Recommended Design Approach for Liquefaction Induced Lateral spreads," *Proc. of 3rd National Seismic Conf. and Workshop on Bridges and Highways*, MCEER-02-SP04, Buffalo, NY.

Mazzoni S, McKenna F, Scott MH and Fenves GL *et al*. (2006), *OpenSees Command Language Manual*, University of California, Berkeley, CA.

Nielson BG and DesRoches R (2007), "Seismic Fragility Methodology for Highway Bridges Using a Component Level Approach," *Earthquake Engineering and Structural Dynamics* **36**: 823–839.

Padgett JE, Nielson BG and DesRoches R (2008), "Selection of Optimal Intensity Measures in Probabilistic Seismic Demand Models of Highway Bridge Portfolios," *Earthquake Engineering and Structural Dynamics*, **37**(5): 711–725.

Priestley MJN, Seible F and Calvi GM (1996), *Seismic Design and Retrofit of Bridges*, John Wiley & Sons, NY.

Shinozuka M, Feng MQ, Lee J and Naganuma T (2000), "Statistical Analysis of Fragility Curves," *Journal of Engineering Mechanics* ASCE, **126**(12): 1224–1231.

United States Geological Survey (USGS) (2007), CPT data Alameda County Online database: http://earthquakeusgsgov/regional/nca/cpt/data/?map=alamed.

Wilson JC (2003), "Repair of New Long-span Bridges Damaged by the 1995 Kobe Earthquake," *Journal of Performance of Constructed Facilities*, **17**(4): 196–205.

Yamazaki F, Motomura H and Hamada T (2000), "Damage Assessment of Expressway Networks in Japan Based on Seismic Monitoring," *Proceedings of 12th World Conference on Earthquake Engineering*, Paper No. 1551, New Zealand.

Yasuda S and Berrill JB (2000), "Observations of the Earthquake Response of Foundations in Soil Profiles Containing Saturated Sands," *Proceeding of GeoEng 2000 Conference*, Melbourne, Australia.

Zhang J and Huo Y (2008), "Optimum Isolation Design for Highway Bridges Using Fragility Function Method," *Proceedings of 14th World Conference on Earthquake Engineering*, Beijing, China.

Zhang J, Huo Y, Kashighandi P and Brandenberg SJ (2008), "Effects of Structural Characterizations on Fragility Functions of Bridges Subjected to Seismic Shaking and Lateral Spreading," *Proceedings of the Sixth National Seismic Conference on Bridges and Highways*, Charleston, S.C.

Zhang J and Makris N (2002a), "Kinematic Response Functions and Dynamic Stiffnesses of Bridge Embankments," *Earthquake Engineering and Structural Dynamics*, **31**: 1933–1966.

Zhang J and Makris N (2002b), "Seismic Response Analysis of Highway Overcrossings including Soil-Structure Interaction," *Earthquake Engineering and Structural Dynamics*, **31**: 1967–1991.